Nanoelectronics and Its New Materials – A NEW ERA OF NANOSCIENCE

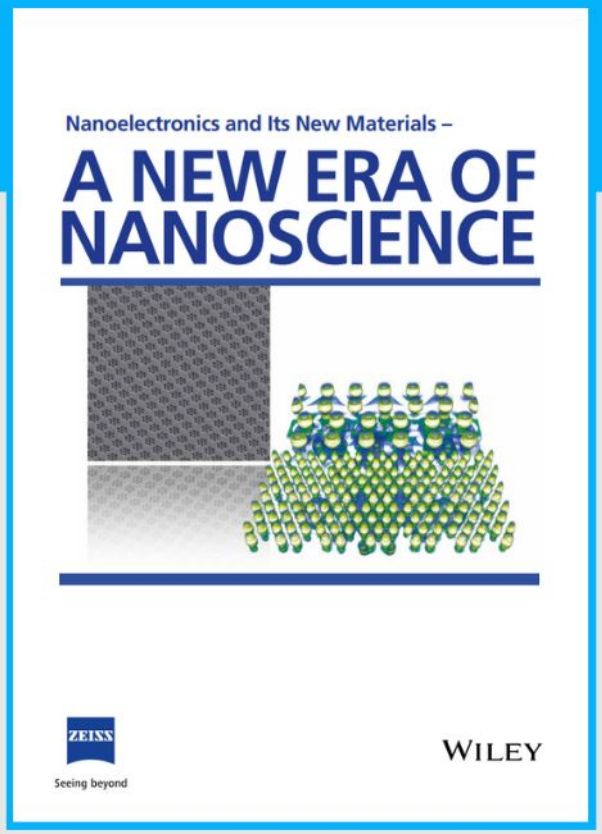

Discover the recent advances in electronics research and fundamental nanoscience.

Nanotechnology has become the driving force behind breakthroughs in engineering, materials science, physics, chemistry, and biological sciences. In this compendium, we delve into a wide range of novel applications that highlight recent advances in electronics research and fundamental nanoscience. From surface analysis and defect detection to tailored optical functionality and transparent nanowire electrodes, this eBook covers key topics that will revolutionize the future of electronics.

To get your hands on this valuable resource and unleash the power of nanotechnology, simply download the eBook now. Stay ahead of the curve and embrace the future of electronics with nanoscience as your guide.

ZEISS

Seeing beyond

WILEY

ADVANCED FUNCTIONAL MATERIALS
www.afm-journal.de

Room-Temperature Phosphorescent Tough Hydrogels Based on Ionically Crosslinked Nonaromatic Polymers

*Junwen Deng, Haiqi Liu, Deyu Liu, Linxuan Yu, Yunhao Bai, Wendi Xie, Tianqi Li, Cuiping Wang, Yifan Lian, and Huiliang Wang**

Organic photoluminescent materials exhibiting room-temperature phosphorescence (RTP) have attracted widespread attention. However, most of them can emit phosphorescence only in the solid state, which strongly limits their applications. Herein, a type of phosphorescent hydrogel with excellent mechanical properties is prepared by immersing an as-prepared poly(vinyl alcohol) (PVA) hydrogel in a poly(sodium maleate) solution and then in a $CaCl_2$ solution, followed by drying under stretching at 90 °C and finally soaking it in deionized water until equilibrium swelling to produce poly(vinyl alcohol)/poly(calcium maleate)-DS (PVA/PMACa-DS) hydrogels. Such hydrogels exhibit excellent mechanical properties, showing tensile strengths up to 15 MPa, due to the presence of strong hydrogen bonding and especially ionic bonding. The PVA/PMACa-DS hydrogels emit varied phosphorescence emission colors from blue to yellow-green upon excitation with 312–400 nm light, with a maximum lifetime of 13.4 ms. Experiments and theoretical calculations demonstrate that ionic crosslinking between Ca^{2+} and nonconventional chromophores prevents the contact of the nonconventional chromophores with water molecules and hence restricts nonradiative decay, leading to RTP emission. This work provides a reliable strategy for designing RTP hydrogels with excellent mechanical properties based on nonaromatic polymers for emerging applications.

1. Introduction

Organic photoluminescent materials exhibiting room-temperature phosphorescence (RTP) have attracted rapidly growing attention because of their wide applications in information encryption,[1,2] bioimaging,[3–5] and optoelectronic devices.[6–8] These compounds are generally comprised of largely extended π-conjugated systems as luminescent chromophores[9,10] and contain heavy atoms (e.g., Br and I) and/or heteroatoms (e.g., N and O) to facilitate intersystem crossing (ISC) between singlet and triplet states.[11–14] Most RTP materials are used in the solid state to suppress molecular motions and reduce the oxygen-mediated nonradiative quenching of the triplet states.[15–17] In contrast, the RTP emission of most phosphorescent materials can be quenched in the aqueous phase due to the presence of dissolved oxygen in it,[18] and the solvent-assisted relaxation.[19,20]

Hydrogels are 3D crosslinked polymer networks that can absorb large amounts of water while maintaining their solid shape.[21–23] The incorporation of photoluminescent materials, such as fluorescent proteins, organic dyes, and lanthanide complexes, into hydrogels produces photoluminescent hydrogels.[24–26] In contrast to solid photoluminescent materials, photoluminescent hydrogels exist as semisolids,[27] combining the unique advantages of both the solid and solution states and hence suggesting excellent potential in a myriad of applications in sensors,[28] bioactuators,[29] and information encoding and encryption.[30]

However, because of the presence of a large amount of water, most photoluminescent hydrogels exhibit only prompt emissions but without obvious RTP.[31,32] It is of paramount importance to prepare phosphorescent hydrogels for exploring applications of organic phosphors in the biological realm.[33] To date, two strategies have been employed to prepare phosphorescent hydrogels: 1) The introduction of phosphorescent metal complexes with in-water phosphorescence emissions. For example, Omary's group incorporated a water-soluble phosphorescent complex $Na_8[Au(TPPTS)_3]$ (TPPTS = tris(3, 3′, 3′′-trisulfonatophenyl) phosphine) into a poly(*N*-isopropylacrylamide) (PNIPAM) network to synthesize a phosphorescent hydrogel with temperature and pH sensitivity.[34] Lovell's group employed Pd-porphyrins as crosslinking points connected by chemical bonds with polyethylene glycol (PEG) polymer chains to generate a hydrogel that exhibits oxygen-responsive phosphorescence.[35] Both hydrogels have maximum phosphorescence lifetimes in the microsecond range. 2) Enhancing physical interactions, such as host–guest, hydrophobic, and electrostatic interactions, to partially isolate the luminescent chromophores from water and rigidify polymer conformations in the hydrogels. For example, Tian's group synthesized a visible-light-excited RTP hydrogel by employing the

J. Deng, H. Liu, D. Liu, L. Yu, Y. Bai, W. Xie, T. Li, C. Wang, Y. Lian, H. Wang
Beijing Key Laboratory of Energy Conversion and Storage Materials
College of Chemistry
Beijing Normal University
Beijing 100875, China
E-mail: wanghl@bnu.edu.cn

The ORCID identification number(s) for the author(s) of this article can be found under https://doi.org/10.1002/adfm.202308420

DOI: 10.1002/adfm.202308420

supramolecular host molecule cucurbit[8]uril (CB)[8] as a confined cavity to incorporate the triazine derivative (TBP).[36] The phosphorescence of the hydrogels could be changed by adjusting the ratio of CB[8] to TBP. Zhao's group introduced a supramolecular complex containing host–guest interactions between CB[8] and allyl-modified 4-(4-bromophenyl) pyridin-1-ium bromide (ABP) into polyvinyl alcohol (PVA)/polyacrylamide (PAAm) hydrogel networks to prepare an RTP hydrogel with a phosphorescence lifetime of 0.9 ms and tensile strength of 110 kPa.[37] George's group recently introduced a phthalimide derivative and Cucurbit[7]uril host–guest system into laponite (LP) clays to prepare a phosphorescent supramolecular hydrogel with a phosphorescence lifetime of 1.34 ms.[38]

The presence of water in hydrogels limits the phosphorescence lifetime of the hydrogels to a few milliseconds or less.[39,40] On the other hand, the incorporation of phosphors into hydrogels can exacerbate the structural inhomogeneity of the gel network, and thus, most reported phosphorescent hydrogels are mechanically very weak.[41] It remains a challenge to prepare phosphorescent hydrogels with long lifetimes and strong mechanical properties, which could greatly broaden their potential applications. Recently, nontraditional luminogens (NTLs) without any aromatic structures have been reported.[42,43] These NTLs contain only electron-rich heteroatoms and/or unsaturated bonds and exhibit strong intrinsic luminescence in the aggregated state when the chromophores are clustered, that is, clustering-triggered emission (CTE).[44–46] NTLs have excellent hydrophilicity and biocompatibility, as well as intrinsic phosphorescent emission, and hence are ideal for the preparation of phosphorescent hydrogels. Up to now, very less attention has been paid to the fabrication of nontraditional phosphorescent hydrogels. Hou et al. prepared anti-freezing poly(acrylamide-*co*-methacrylic acid) hydrogels with dense hydrogen-bond associations, which lead to the formation of carbonyl clusters and hence could emit phosphorescence at subzero temperatures.[47] Very recently, Wu's group reported a novel type of crown ethers-polyacrylamide (CEs-PAAm) hydrogel with persistent RTP emission. The polymerization of PAAm induces the crystallization of crown ethers in the hydrogel, which facilitates the clusterization and confinement of nonconventional chromophores in PAAm, leading to the origination of RTP.[48] However, the presence of crystallization of CEs exacerbates the structural inhomogeneity of the gel network, and hence such CEs-PAAm gel processes weak mechanical properties with breaking stress of 166 kPa. Therefore, preparing phosphorescent hydrogels especially nontraditional phosphorescent hydrogels with both high mechanical properties and obvious RTP emission is a challenge of great significance for the promising applications of phosphorescent materials and phosphorescent hydrogels.

In this work, we prepared a nonaromatic phosphorescent hydrogel, poly(vinyl alcohol) (PVA)/poly(calcium maleate) (PMACa)-DS (PVA/PMACa-DS), where "DS" means the drying under stretching and equilibrium swelling (**Figure 1**a). The PVA/PMACa-DS hydrogels show excellent mechanical properties, with a tensile strength of up to 15 MPa at a water content of 67.6%. Moreover, PVA/PMACa-DS hydrogels exhibit varied phosphorescent emission colors upon excitation with 312–400 nm light, with a maximum lifetime of 13.4 ms. The mechanism of RTP and its high mechanical properties were investigated by comparative studies and theoretical calculations.

2. Results and Discussion

2.1. Preparation and Characterization of PVA/PMACa-DS Hydrogels

The preparation process of PVA/PMACa-DS hydrogels is shown in Figure 1a. First, PVA hydrogels were prepared by the classical freezing-thawing (F-T) method. During the F-T process, partial PVA chains form crystallites that do not melt when thawed at room temperature and function as cross-linking points to connect the PVA chains. Then, these PVA hydrogels were directly immersed in a poly(sodium maleate) (PMANa) aqueous solution to obtain PVA/PMANa hydrogels. The osmotic pressure difference between the PVA hydrogel and the PMANa solution drives the diffusion of short PMANa chains from the solution into the hydrogel. Then, the as-prepared PVA/PMANa hydrogels were immersed in a calcium chloride aqueous solution to induce the formation of ionic crosslinks between the polymer chains and Ca^{2+}. Next, the PVA/PMACa hydrogels were stretched to 150% of their original strain and dried under stretching in the air at 90 °C. The drying under stretching is effective in forming more hydrogen bonds and ionic bonds in the hydrogels.[49] Finally, the dried gels were immersed in water to reach equilibrium swelling, and PVA/PMACa-DS hydrogels were obtained (Figure S1, Supporting Information). The water contents of the hydrogels are provided in Table S1, Supporting Information.

X-ray photoelectron spectroscopy (XPS) analysis proves that a significant amount of PMANa has been introduced into the PVA hydrogel, as indicated by the appearance of carboxyl C (O—C═O, 288 eV) peak in the spectrum of PVP/PMANa hydrogel in addition to carbons of PVA (C—C and C—O) (Figure 1b,c). The introduction of the carboxyl group (6.5%) leads to an increase in the proportion of C—C but a decrease in the proportion of C—O in the PVP/PMANa hydrogel with comparison to those in the PVA hydrogel. The content of Ca^{2+} in the PVA/PMACa-DS hydrogels is 5.7 wt%. X-ray diffraction (XRD) profiles of PVA, PVA/PMANa, PVA/PMACa, and PVA/PMACa-DS hydrogels are shown in Figure 1d. A sharp crystalline peak at $2\theta = 19.31°$ ($d = 4.58$ Å) and a shoulder peak at $2\theta = 22.61°$ ($d = 3.93$ Å) corresponding to the (101_) and (200) planes of PVA crystallites are observed for all the hydrogels, suggesting that the PVA crystallites are present in all samples.[50] The calculated degree of crystallinity (X_c) value of the PVA hydrogel is 42%, while the X_c values of the PVA/PMANa and PVA/PMACa hydrogels decrease to ≈36% due to the introduction of amorphous PMANa. However, the X_c of the PVA/PMACa-DS hydrogel increases to 61.6%, confirming that the drying under the stretching process could promote the crystallization of PVA.[51] The polarized optical microscope (POM) images of the PVA/PMACa hydrogel show randomly distributed bright and dark regions at different rotation angles, while the PVA/PMACa-DS hydrogel is very bright at the rotation angles of 0° and 90°, but it becomes darker at a rotation angle of 45°, indicating the presence of oriented crystalline structures (Figure 1e).

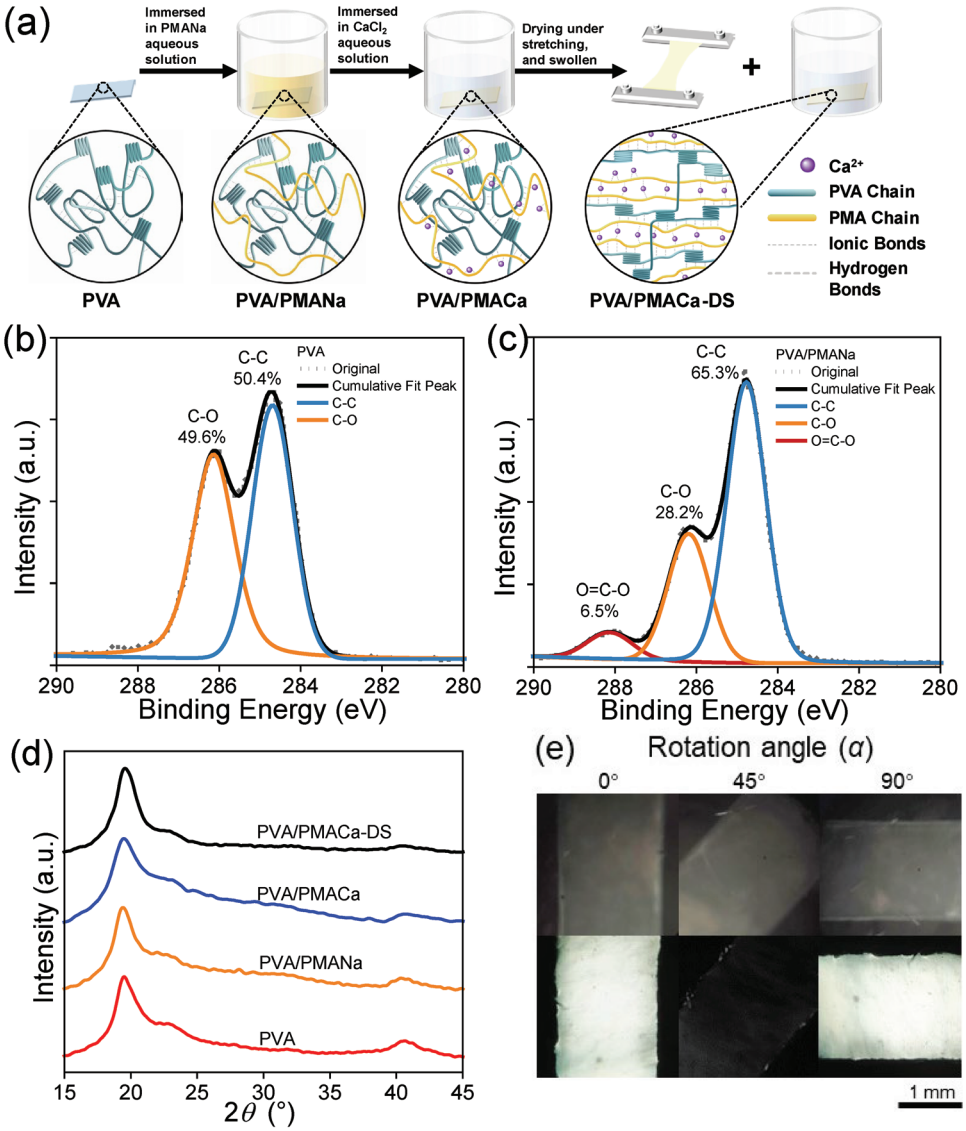

Figure 1. a) Schematic illustration of the preparation process and physical interactions in the PVA, PVA/PMANa, PVA/PMACa, and PVA/PMACa-DS hydrogels. b,c) Curve-fitted C_{1s} XPS spectra of the cross-section of b) PVA hydrogel and c) PVA/PMANa hydrogel. d) X-ray diffraction (XRD) profiles of PVA, PVA/PMANa, PVA/PMACa, and PVA/PMACa-DS hydrogels. e) Polarized optical microscopy (POM) images of the PVA/PMACa (upper) and PVA/PMACa-DS (lower) hydrogel at different rotation angles.

2.2. Mechanical Properties of the PVA/PMACa-DS Hydrogels

Figure 2a,b shows the tensile mechanical properties of the PVA, PVA/PMANa, PVA/PMACa, and PVA/PMACa-DS hydrogels. The PVA hydrogel possesses a tensile strength (σ_b), elastic modulus (E), and toughness (K) of 0.42 MPa, 0.02 MPa, and 0.79 MJ m^{-3}, respectively, while the PVA/PMANa and PVA/PMACa hydrogels exhibit slightly improved σ_b, E, and K. The PVA/PMACa-DS hydrogel exhibits dramatically enhanced mechanical properties with a σ_b, E, and K of ≈15 MPa, 2.41 MPa, and 45.2 MJ m^{-3}, respectively. The PVA/PMACa-DS hydrogel string with a diameter of 0.5 mm can withstand a load of 2.5 kg (Figure 2e).

Rheological measurements were carried out to understand the viscoelastic responses of the PVA, PVA/PMANa, PVA/PMACa, and PVA/PMACa-DS hydrogels. When the shear strain is less than 0.1%, the storage modulus (G') is much larger than the loss modulus (G''), and the loss factor ($\tan\delta$) is less than 0.06, indicating the elastic solid nature of the gels (Figure 2c and Figure S2, Supporting Information). That is, when the deformation is sufficiently small, the molecular structure of the physical crosslinked hydrogels remains close to equilibrium, and the crosslinking structure remains intact. However, at higher shear strains, the hydrogels exhibit nonlinear viscoelastic behavior. G' decreases by ≈3 orders of magnitude as γ increases from 0.1% to 100% strain, and G'' exhibits a maximum at γ = 1% for PVA and PVA/PMANa and γ = 3% for the PVA/PMACa and PVA/PMACa-DS hydrogels. The peak in G'' indicates a transition where energy is dissipated (viscous response), and the change in the mechanical properties to $G'' > G'$ signifies a transition

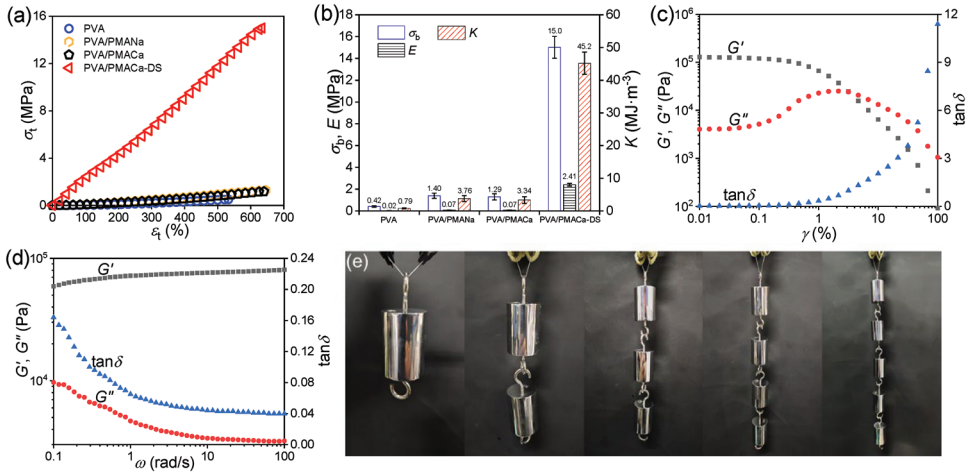

Figure 2. a,b) Typical tensile stress–strain (σ_t–ϵ_t) curves (a), tensile strength (σ_b), toughness (K), and Young's modulus (E) (b) of the PVA, PVA/PMANa, PVA/PMACa, and PVA/PMACa-DS hydrogels. c,d) Storage modulus (G'), loss modulus (G''), and loss factor (tanδ) as a function of shear strain (γ) (c) and frequency (ω) (d) for the PVA/PMACa-DS hydrogels. e) Photographs of the PVA/PMACa-DS hydrogel sample with a 0.5 mm diameter withstanding loads of 0.5 to 2.5 kg.

from solid to viscous fluid. Note that the shift of the G'''' peak for PVA/PMACa and PVA/PMACa-DS to higher shear strains can be attributed to crosslinking between polymer chains with Ca^{2+}. Following that transition, the further decrease in G'' and G', as well as the increase in tanδ , indicate that the viscosity and elasticity of the liquid decrease with increasing strain amplitude. Figure 2d shows the frequency dependence of the G', G'', and tanδ of the PVA/PMACa-DS hydrogels. With increasing frequency, G' increases, but G'' and tanδ decreases, showing a significant frequency dependence. These rheological test results suggest the physical crosslinking nature of the hydrogels.

2.3. Photoluminescence of the PVA/PMACa-DS Hydrogel

The PVA/PMACa-DS hydrogel exhibits remarkable excitation-dependent fluorescence and phosphorescence emissions. Upon the irradiation at 312, 365, and 400 nm lights, the PVA/PMACa-DS hydrogel shows blue, cyan, and green prompt emissions, respectively. Note that 400 nm violet light is visible, and the strong background causes overexposure of the photograph. After turning off the lights, the samples emit deep blue, blue-green, and greenish-yellow RTP, corresponding to maximum emission wavelengths (λ_{em}^{max}) at 460, 470, and 495 nm, respectively (**Figure 3**a,b) with the maximum phosphorescence lifetime at 13.4 ms (Figure 3c). The obtained hydrogels immersed in the $CaCl_2$ aqueous solution at different times show RTP with the same λ_{em}^{max} (Figures S3 and S4, Supporting Information). The PL intensity and lifetime of the delayed emissions increase with the decrease in temperature (Figure S5, Supporting Information), indicating that the delayed emission from the PVA/PMACa-DS hydrogel is phosphorescence rather than delayed fluorescence. More importantly, the PVA/PMACa-DS hydrogel also exhibits the same RTP in water as in air (Figure 3a, right), and has stable phosphorescent emission intensity within 50 UV light irradiation/recovery cycles (Figure S6, Supporting Information). Therefore, PVA/PMACa-DS hydrogels can potentially be used in biomaterials and in-water actuators.

2.4. RTP Mechanism of the PVA/PMACa-DS Hydrogel

To understand the phosphorescence mechanism of the PVA/PMACa-DS hydrogel, the photoluminescence behaviors of the PVA, PVA/PMANa, and PVA/PMACa hydrogels were investigated. The hydrogels are all white under natural light (**Figure 4**a) and exhibit prompt emissions under the irradiation of 312 nm UV light. From the PVA/PMANa to PVA/PMACa hydrogels, the λ_{em}^{max} red-shifts from 401 to 450 nm (Figure S7, Supporting Information). After turning off the light source, only the PVA/PMACa hydrogel emits blue phosphorescence. The delayed emission spectra of the PVA/PMACa and PVA/PMANa hydrogels, as well as the dried gels (xerogels) of PVA/PMANa (PVA/PMANa-X) are shown in Figure 4b. The PVA/PMANa hydrogel exhibits only prompt emission but no phosphorescence emission (Figure S8, Supporting Information), while the PVA/PMANa-X exhibits phosphorescence emission with a similar λ_{em}^{max} as those of the PVA/PMACa and PVA/PMACa-DS hydrogels at about 465 nm (Figure 4c, and Figures S9 and S10, Supporting Information). In addition, the PVA/PMACa-DS xerogel (PVA/PMACa-DS-X) also exhibits phosphorescence with the λ_{em}^{max} as that of the PVA/PMACa-DS hydrogel, but it has a much longer lifetime of 121.1 ms than that of PVA/PMACa-DS hydrogel (Figure 4b,c). The above results suggest that the presence of water in the hydrogels induces the hydration of chromophores and the breakage of hydrogen bonds between adjacent chromophores, which leads to the enhanced molecular motion and nonradiative decay and hence the quenching or decrease of phosphorescence emissions without changing the emission wavelengths.[52] In addition, the drying under stretching method also does not change the emission wavelengths of the hydrogel, but the formation of strong hydrogen bonding and ionic bonding in the oriented structures of the PVA/PMACa-DS hydrogel

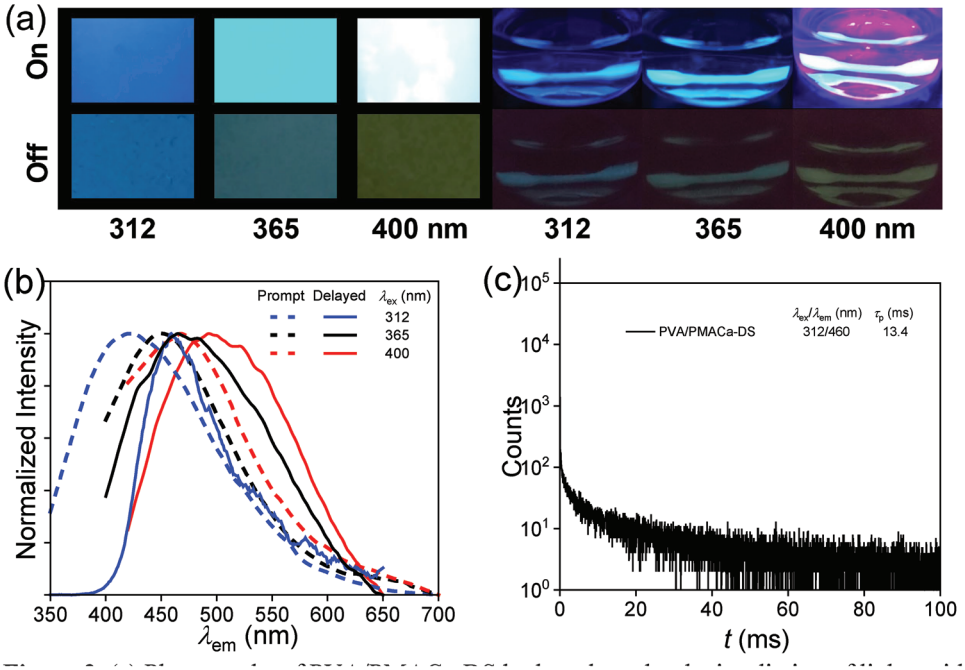

Figure 3. a) Photographs of PVA/PMACa-DS hydrogels under the irradiation of lights with different wavelengths and after ceasing the irradiation for 0.1 s in air (left) and water (right). b,c) Prompt (dashed line) and delayed emission (solid lines, t_d = 1 ms) spectra (b), as well as lifetime profiles (c) of the PVA/PMACa-DS hydrogel.

resists the movement of polymer chains and hence inhibits the nonradiative decay, leading to an increased phosphorescence lifetime.

The photoluminescence behaviors of the PVACa hydrogel and PMACa solid powders were also comparatively tested to investigate the photoluminescent species in the PVA/PMACa-DS hydrogel. The PMACa powders exhibit phosphorescence with λ_{em}^{max}at 485, 545, and 555 nm upon excitations at 312, 365, and 400 nm, respectively (Figure 4d and Figure S11, Supporting Information) which are significantly red-shifted with comparison to those of the PVA/PMACa-DS hydrogel and the PVA/PMACa-DS-X gel. The lifetime profile of PMACa powders is shown in Figure 4c. PMACa powders have a phosphorescence lifetime of 100.2 ms, shorter than that of PVA/PMACa-DS-X (121.1 ms). Moreover, the quantum yield of PMACa powders (6.2%) is lower than that of PVA/PMACa-DS-X gel (8.2%) (Table S2, Supporting Information). These results suggest that the interactions between PVA and PMACa chains in PVA/PMACa-DS-X could rigidify their conformations and hence enhance the photoluminescence emission.

On the other hand, the PVACa hydrogel shows no phosphorescence emission and its prompt emission is blue-shifted compared to that of the PVA/PMACa-DS hydrogel (Figure 4e). Therefore, the photoluminescence emissions of the PVA/PMACa-DS hydrogel and the PVA/PMACa hydrogel originate from the through-space conjugation of PVA and PMACa chains rather than from a single luminescent species in the hydrogels.

Theoretical calculations were performed to optimize the excited-state structures and simulate the frontier molecular orbitals of PVA/PMACa-X. The electron clouds of the highest occupied molecular orbital (HOMO) of dried PVA/PMACa are distributed on both the PVA and PMA chains, while those of the lowest unoccupied molecular orbital (LUMO) are localized only on the PMA chain, proving the occurrence of through-space conjugation between the PVA and PMACa chains (**Figure 5**a), which could rigidify the conformations of polymer chains. In addition, the spin-orbit coupling (SOC) constant ($\xi_{S1\text{-}T1}$) of the PVA/PMACa-X is as high as 11.74 cm^{-1}, suggesting that the ISC transition from the S_1 to T_1 state is easy to occur. The distance between the oxygen atoms on adjacent chains in the PVA/PMACa-X is ≈3.1 Å, suggesting the presence of strong through-space interactions between polymer chains (Figure 5b and Table S3, Supporting Information). To simulate the water-containing environment of the hydrogels, eight water molecules were added to the system for molecular optimization. Compared to the PVA/PMACa-X, the PVA/PMACa hydrogel has a similar $d_{o\text{-}o}$, while in the PVA/PMANa hydrogel, the distances between oxygen atoms are significantly increased due to the hydration of carboxyl and hydroxyl groups (Figure 5c and Tables S4 and S5, Supporting Information). Based on the theoretical calculations and experimental results, it is confirmed that the introduction of calcium ions enhances the cross-linking between polymer chains in the hydrogels. The strong interactions between PVA and PMACa chains prevent the contact of nonconventional chromophores with water and restrict their nonradiative decay, leading to the phosphorescence emission of the PVA/PMACa and PVA/PMACa-DS hydrogels.

In addition, PVA/poly(zinic maleate) (PMAZn)-DS and PVA/poly(barium meleate) (PMABa)-DS hydrogels were also prepared and they exhibit similar mechanical and photophysical properties as those of the PVA/PMACa-DS hydrogels (Figures S12 and S13, Supporting Information), suggesting that the

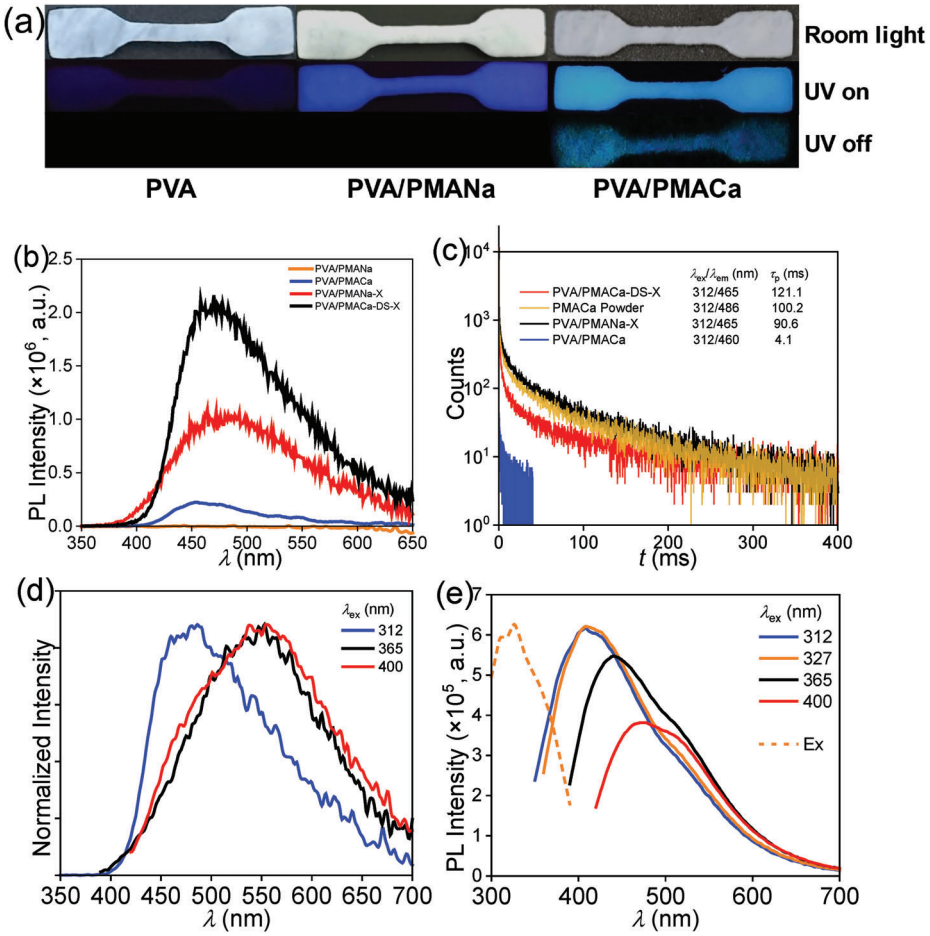

Figure 4. a) Photographs of the PVA, PVA/PMANa, and PVA/PMACa hydrogels under room light and 312 nm UV irradiation and after the ceasing of irradiation for 1/30 s in air. b) Delayed emission spectra of the PVA/PMANa hydrogel, PVA/PMACa hydrogel, PVA/PMANa-X gel, and PVA/PMACa-DS-X gel (λ_{ex} = 312 nm, t_d = 1 ms). c) Lifetime profiles of the PVA/PMACa-DS-X gel, PMACa solid powders, PVA/PMANa-X gel, and PVA/PMACa hydrogel. d) Delayed emission spectra of the PMACa solid powders (t_d = 1 ms). e) Prompt excitation (dashed line, λ_{em} = 408 nm) and emission (solid lines) spectra of the PVACa dried gels.

strategy in this work is reliable to produce phosphorescent hydrogels with high mechanical properties.

3. Conclusion

In summary, we fabricated a novel type of nontraditional phosphorescent PVA/PMACa-DS hydrogels with a long lifetime and extraordinary mechanical properties. The sequential introduction of poly(sodium maleate) (PMANa) and Ca^{2+} into a PVA hydrogel and the drying under stretching process leads to the formation of strong ionic bonding and hydrogen bonding in the oriented structures in the hydrogel, which significantly improves the mechanical properties. More importantly, the PVA/PMACa-DS hydrogel emits excitation-dependent RTP with a maximum lifetime of 13.4 ms. Experiments and theoretical calculations prove that the interactions between polymer chains and Ca^{2+} cations in the PVA/PMACa-DS hydrogel prevent the contact of nonconventional chromophores with water molecules and could rigidify the conformations of polymer chains. Therefore, the nonradiative decay of nonconventional chromophores is inhibited, leading to the phosphorescence emission of the PVA/PMACa-DS hydrogel. In this work, a novel and reliable strategy for preparing nontraditional phosphorescent hydrogels with good mechanical properties is provided, and it may greatly expand the practical applications of photoluminescent hydrogels.

4. Experimental Section

Materials: PVA ($M_n \approx 7.7 \times 10^4$, 98% alcoholysis degree) was purchased from Sinopharm Chemical Reagent Co., Ltd. (Beijing, China). Poly(maleic acid) (PMA, $M_w \approx 5.7 \times 10^3$, $M_n \approx 2.8 \times 10^3$) aqueous solution (50 wt%) was purchased from Shanghai Macklin Biochemical Co., Ltd. Anhydrous calcium chloride ($CaCl_2$), zinc chloride ($ZnCl_2$), barium chloride ($BaCl_2$), and sodium hydroxide (NaOH) were obtained from Beijing Chemical Works Co., Ltd. (Beijing, China). All chemicals were of AR grade and were used as received without further purification. Deionized water was used for all experiments.

Preparation of PVA Hydrogels: PVA (14 g) was dissolved in 86 g of deionized water under continuous mechanical stirring at 110 °C until a

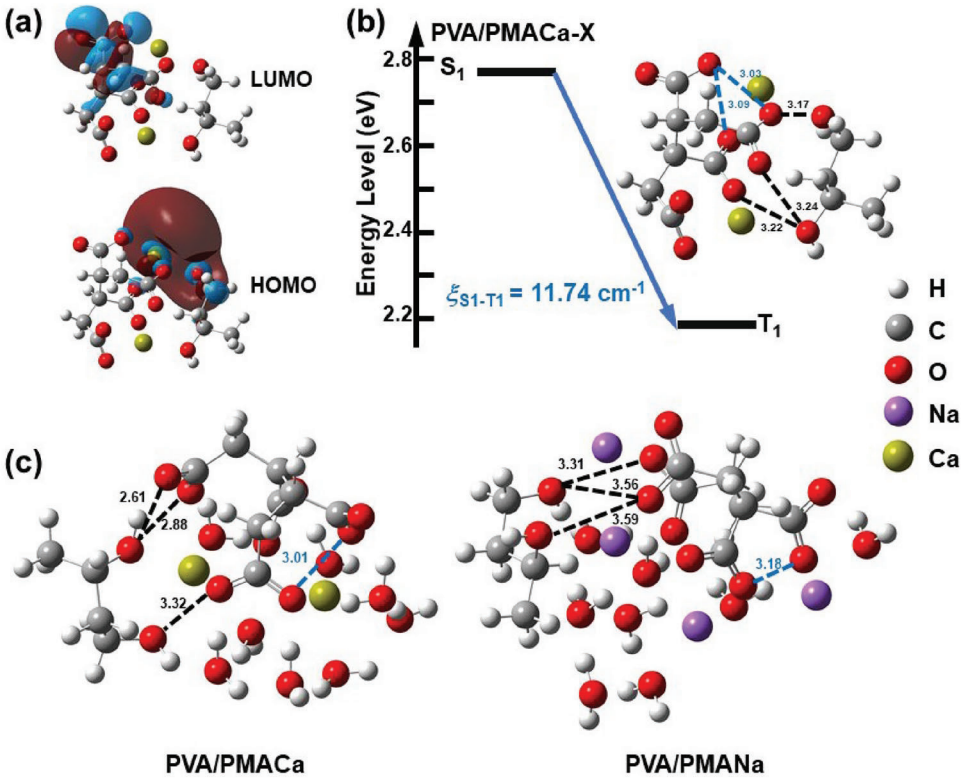

Figure 5. a) Schematic diagram of the HOMO and LUMO orbitals of the PVA/PMACa-X. b) Energy levels of excited singlets, $\xi_{S1\text{-}T1}$, and optimized molecular structures of the PVA/PMACa-X. c) Optimized molecular structures of the PVA/PMACa and PVA/PMANa hydrogels.

clear and homogeneous aqueous solution was obtained. After cooling to 65 °C, the PVA solution (14 wt%) was transferred into a mold composed of two glass plates (10 cm × 10 cm) and a silicone frame (thickness: 1 mm). Then it was frozen at −23 °C for 24 h and thawed at 4 °C for 12 h.

Preparation of PVA/Poly(Sodium Maleate) (PMANa), PVA/Poly(Zinc Maleate) (PMAZn), PVA/Poly(Barium Maleate) (PMABa), and PVA/Poly(Calcium Maleate) (PMACa) Hydrogels: A PMANa aqueous solution was prepared by reacting an aqueous solution of PMA with a NaOH aqueous solution (1.25 mol L^{-1}). The PVA hydrogels were immersed in a 50 g L^{-1} PMANa aqueous solution to obtain PVA/PMANa hydrogels. Then, the PVA/PMANa hydrogels were immersed in 0.1 mol L^{-1} chlorides ($ZnCl_2$, $BaCl_2$, or $CaCl_2$) aqueous solutions for 4 h to obtain PVA/PMAZn, PVA/PMABa, and PVA/PMACa hydrogels, respectively.

Preparation of PVA/PMAZn-DS, PVA/PMABa-DS, and PVA/PMACa-DS Hydrogels: The PVA/PMAZn, PVA/PMABa, and PVA/PMACa hydrogels were stretched to 150% of their original strain and dried under stretching in the air at 90 °C. Then, the dried hydrogels were swollen in deionized water at room temperature to equilibrium swelling, and then PVA/PMAZn-DS, PVA/PMABa-DS, and PVA/PMACa-DS hydrogels were obtained, respectively.

Preparation of Samples Used in Rheological Measurements: The classical F-T method was employed to prepare PVA hydrogels with a thickness of 5 mm. By immersing the PVA hydrogels in a PMANa solution and then in a $CaCl_2$ solution, PVA/PMANa and PVA/PMACa hydrogels with a thickness of about 5 mm were prepared. After the drying under stretching and equilibrium swelling process mentioned above, PVA/PMACa-DS hydrogels with a thickness of about 2 mm were obtained and used for rheological measurements. These hydrogels were cut into disc sheets with a diameter of 25 mm and then fixed on a parallel plate.

Characterization: Fourier transform infrared (FT-IR) spectra of the samples were recorded with a Nicolet iS 50 spectrometer (Thermo Electron Corporation, USA), and the number of scans was 32 at a resolution of 1 cm^{-1}. XPS measurements were recorded on a multifunctional X-ray photoelectron spectrometer (Axis Ultra, Kratos Analytical Ltd, England) with Al K_α radiation and low energy electron streams as the excitation source (225 W, 15 mA, 15 kV). XRD was performed using an X-ray diffractometer (PANalytical Co. Ltd, Netherlands) equipped with a Ni-filtered Cu K_α radiation (λ = 1.542 Å) source. The oriented structures of the PVA/PMACa and PVA/PMACa-DS hydrogels were observed by using a POM (OPTEC, SMART-POL, China) equipped with a high-quality SLR camera (Canon, EOS600D, Japan) in transmission mode in a cross-polarized configuration.

Measurement of Water Contents: The equilibrium water content (EWC) of hydrogel samples was calculated by Equation (1)

$$\text{EWC}\ (\%) = \frac{m_{\text{wet}} - m_{\text{dry}}}{m_{\text{wet}}} \times 100 \quad (1)$$

where m_{wet} is the mass of swollen samples and m_{dry} is the mass of dried samples. Their average values and deviations were calculated.

Tensile Tests: The tensile mechanical properties of the hydrogels were determined by using an Instron 3366 electronic testing machine (Instron Corporation, USA) with a 100 N load cell at a cross-head speed of 100 mm min^{-1}. The dimensions of the dumbbell-shaped hydrogel specimens were standardized as DIN 53 504 S3, that is, overall length: 35 mm; gauge length: 10 mm; width: 2 mm; and inner width: 1 mm.

The tensile stress (σ_t) was calculated using the following equation

$$\sigma_t = \frac{\text{Load}}{S} \quad (2)$$

where S is the cross-sectional area of the specimen and σ_t is referred to as nominal stress. Tensile strain (ϵ_t) is defined as the change in the length relative to the gauge length of a freestanding specimen. The tensile strength

(σ_b) and strain (ϵ_b) are the tensile stress and strain at which the specimen breaks, respectively. Initial tensile elastic modulus (E) was calculated from the linear stress–strain relationship in the strain range of 10–30%. At least five specimens per experimental point were tested to guarantee the reliability of the data.

Toughness (K) was characterized as the area surrounded by the stress (σ)–strain (ϵ) curves using Equation (3)

$$K \left(\mathrm{KJ\ m^{-3}}\right) = \int_{\varepsilon=0}^{\varepsilon=\varepsilon_{max}} \sigma d\varepsilon \quad (3)$$

where σ is the stress (MPa) and ϵ is the strain (mm mm^{-1}).

Rheological Measurements: Linear and nonlinear oscillatory shear measurements were performed with an MCR 302 rheometer (Anton Paar, Austria) equipped with 8 mm parallel plates and a solvent trap filled with silicone oil to minimize water evaporation. The linear viscoelastic (LVE) response region for each sample was determined at $T = 25$ °C using a strain sweep from $\gamma = 0.1\%$ to 100% at a constant frequency, $\omega = 0.1$ rad s^{-1}. Frequency-dependent LVE data were obtained at $T = 25$ °C and a strain amplitude of $\gamma = 0.1\%$ over a frequency range of 0.01–100 rad s^{-1}.

Photoluminescence Spectroscopy: Photoluminescent emission and excitation spectra, as well as fluorescence and phosphorescence lifetimes, were measured with an FLS-980 photoluminescent spectrometer (Edinburgh Instruments, UK). Photoluminescence quantum yields were measured with an Absolute PL Quantum Yield Spectrometer (Quantaurus-QY, Hamamts, Japan). Measurements of photoluminescence were all carried out in air at ambient temperature if not otherwise stated. Photographs of the hydrogel samples under the irradiation of UV light of different wavelengths were taken with a Nikon D7100 digital camera in a dark room. The photographs of delayed emissions of hydrogels were taken after turning off the lights for 0.1 and 1/30 s in Figures 3a and 4a, respectively.

ICP-AES Analysis: The PVA/PMACa-DS hydrogels were reacted with concentrated HNO_3 to form water-soluble $Ca(NO_3)_2$, and then the diluted aqueous $Ca(NO_3)_2$ solutions were measured by inductively coupled plasma atomic emission spectroscopy (ICP-AES) on a SPECTRO ARCOS EOP instrument (SPECTRO Analytical Instruments GmbH, Germany).

Theoretical Calculations: All conformational scans are performed by ABCluster, a code proposed by Zhang and Dolg.[53–55] Conformation (structure) optimizations were performed with density functional theory (DFT) and time-dependent density functional theory (TD-DFT) on the basis of Gaussian 16 software (version A.03).[56] The SOC matrix elements between singlet and triplet states were evaluated through ORCA (version 5.0.0).[57] Conformations with and without water were calculated using PBE0/6-31 g and PBE0/def2svp levels, respectively.[58–64] None of the optimized conformations contained imaginary frequencies. The HOMO-LUMO electron cloud distribution and electrostatic potential maps were plotted with GaussView 6.0.

Supporting Information

Supporting Information is available from the Wiley Online Library or from the author.

Acknowledgements

The authors are grateful for financial support from the National Natural Science Foundation of China (Grant Nos. 21574015, 21875023) and the Program for Changjiang Scholars and Innovative Research Team (PCSIRT) at the University.

Conflict of Interest

The authors declare no conflict of interest.

Data Availability Statement

Research data are not shared.

Keywords

high mechanical strength, hydrogels, metal cation crosslinking, nontraditional luminescence, room-temperature phosphorescence

Received: July 20, 2023
Revised: August 28, 2023
Published online:

[1] K. Jiang, Y. Wang, C. Cai, H. Lin, *Adv. Mater.* **2018**, *30*, 1800783.
[2] Y. Su, S. Z. F. Phua, Y. Li, X. Zhou, D. Jana, G. Liu, W. Q.i Lim, W. K. Ong, C. Yang, Y. Zhao, *Sci. Adv.* **2018**, *4*, eaas9732.
[3] S. M. A. Fateminia, Z. Mao, S. Xu, Z. Yang, Z. Chi, B. Liu, *Angew. Chem., Int. Ed.* **2017**, *56*, 12160.
[4] Q. Miao, C. Xie, X.u Zhen, Y. Lyu, H. Duan, X. Liu, J. V. Jokerst, K. Pu, *Nat. Biotechnol.* **2017**, *35*, 1102.
[5] J. Yang, X.u Zhen, B. Wang, X. Gao, Z. Ren, J. Wang, Y. Xie, J. Li, Q. Peng, K. Pu, Z. Li, *Nat. Commun.* **2018**, *9*, 840.
[6] B. Song, W. Shao, J. Jung, S.-J. Yoon, J. Kim, *ACS Appl. Mater. Interfaces* **2020**, *12*, 6137.
[7] Z. Chen, M. Li, Q. Gu, X. Peng, W. Qiu, W. Xie, D. Liu, Y. Jiao, K. Liu, J. Zhou, S.-J. Su, *Adv. Sci.* **2023**, *10*, 2207003.
[8] T. Wang, X. Su, X. Zhang, X. Nie, L. Huang, X. Zhang, X. Sun, Y.i Luo, G. Zhang, *Adv. Mater.* **2019**, *31*, 1904273.
[9] L. Gu, H. Shi, L. Bian, M. Gu, K. Ling, X. Wang, H. Ma, S. Cai, W. Ning, L. Fu, H.e Wang, S. Wang, Y. Gao, W. Yao, F. Huo, Y. Tao, Z. An, X. Liu, W. Huang, *Nat. Photonics* **2019**, *13*, 406.
[10] G. M. Russell, D. Inamori, H. Masai, T. Tamaki, J. Terao, *Polym. Chem.* **2019**, *10*, 5280.
[11] G. Baryshnikov, B. Minaev, H. Ågren, *Chem. Rev.* **2017**, *117*, 6500.
[12] C. M. Marian, *WIREs: Comput. Mol. Sci.* **2012**, *2*, 187.
[13] L. Ma, X. Ma, *Sci. China Chem.* **2023**, *66*, 304.
[14] T. Zhu, T. Yang, Q. Zhang, W. Z. Yuan, *Nat. Commun.* **2022**, *13*, 2658.
[15] A. Qin, *Sci. China Chem.* **2018**, *61*, 635.
[16] Y. Gong, Y. Tan, J.u Mei, Y. Zhang, W. Yuan, Y. Zhang, J. Sun, B. Z. Tang, *Sci. China Chem.* **2013**, *56*, 1178.
[17] E. Hamzehpoor, D. F. Perepichka, *Angew. Chem., Int. Ed.* **2020**, *59*, 9977.
[18] M. Singh, K. Liu, S. Qu, H. Ma, H. Shi, Z. An, W. Huang, *Adv. Opt. Mater.* **2021**, *9*, 2002197.
[19] A.-Y. Ni, B.-L. Zhang, P.-P. Zhang, J.-J. Zhang, H.-Y. Wang, K.-X. Feng, S. Liu, J. Ni, C. Duan, *Dyes Pigm.* **2023**, *210*, 110959.
[20] Q. Li, M. Zhou, M. Yang, Q. Yang, Z. Zhang, J. Shi, *Nat. Commun.* **2018**, *9*, 734.
[21] B. Han, C. Cao, A. Wang, Y. Zhao, M. Jin, Y. Wang, S. Chen, M. Yu, Z. Yang, X. Qu, X. Wang, *ACS Appl. Mater. Interfaces* **2023**, *15*, 7821.
[22] H. Fan, J. Wang, J. P. Gong, *Adv. Funct. Mater.* **2021**, *31*, 2009334.
[23] X. N. Zhang, Q. Zheng, Z. i L. Wu, *Composites, Part B* **2022**, *238*, 109895.
[24] M. X. Wang, C. H. Yang, Z. Q.i Liu, J. Zhou, F. Xu, Z. Suo, J. H. Yang, Y. M. Chen, *Macromol. Rapid Commun.* **2015**, *36*, 465.
[25] A. M. Breul, M. D. Hager, U. S. Schubert, *Chem. Soc. Rev.* **2013**, *42*, 5366.
[26] S. Lyu, J. Fang, T. Duan, L. Fu, J. Liu, H. Li, *Chem. Commun.* **2017**, *53*, 13375.
[27] H. Qiu, S. Wei, H. Liu, B. Zhan, H. Yan, W. Lu, J. Zhang, S.i Wu, T. Chen, *Adv. Intell. Syst.* **2021**, *3*, 2000239.

[28] Y. Yu, M. S. Kwon, J. Jung, Y. Zeng, M. Kim, K. Chung, J. Gierschner, J. i H. o Youk, S. M. Borisov, J. Kim, *Angew. Chem., Int. Ed.* **2017**, *56*, 16207.
[29] X. Le, W. Lu, J. Zhang, T. Chen, *Adv. Sci.* **2019**, *6*, 1801584.
[30] G. Su, Z. Li, J. Gong, R. Zhang, R. Dai, Y. Deng, B. Z. Tang, *Adv. Mater.* **2022**, *34*, 2207212.
[31] J. Deng, H. Wu, W. Xie, H. Jia, Z. Xia, H. Wang, *ACS Appl. Mater. Interfaces* **2021**, *13*, 39967.
[32] Y. Zhang, X. Le, Y. Jian, W. Lu, J. Zhang, T. Chen, *Adv. Funct. Mater.* **2019**, *29*, 1905514.
[33] J. Wang, A. Li, Z. Li, *Prog. Chem.* **2022**, *34*, 487.
[34] S. Marpu, Z. Hu, M. A. Omary, *Langmuir* **2010**, *26*, 15523.
[35] H. Huang, W. Song, G. Chen, J. M. Reynard, T. Y. Ohulchanskyy, P. N. Prasad, F. V. Bright, J. F. Lovell, *Adv. Healthcare Mater.* **2014**, *3*, 891.
[36] J. Wang, Z. Huang, X. Ma, H.e Tian, *Angew. Chem., Int. Ed.* **2020**, *59*, 9928.
[37] Y. Zhou, D.i Zhao, Z.i-Y.i Li, G.e Liu, S.u-H. Feng, B.-T. Zhao, B.-M. Ji, *Dyes Pigm.* **2021**, *195*, 109725.
[38] S. Garain, B. C. Garain, M. Eswaramoorthy, S. K. Pati, S. J. George, *Angew. Chem., Int. Ed.* **2021**, *60*, 19720.
[39] T. Zhang, X. Ma, H.e Tian, *Chem. Sci.* **2020**, *11*, 482.
[40] H. Chen, X. Ma, S. Wu, H.e Tian, *Angew. Chem., Int. Ed.* **2014**, *53*, 14149.
[41] X. Jiang, M. Wu, L.u Zhang, J. Wang, M. Cui, J. Wang, X. Pang, B. Song, Y. He, *Anal. Chem.* **2022**, *94*, 7264.
[42] W. Zhang Yuan, Y. Zhang, *J. Polym. Sci., Part A: Polym. Chem.* **2017**, *55*, 560.
[43] D. A. Tomalia, B. Klajnert-Maculewicz, K. A.-M. Johnson, H. F. Brinkman, A. Janaszewska, D. M. Hedstrand, *Prog. Polym. Sci.* **2019**, *90*, 35.
[44] S. Tang, T. Yang, Z. Zhao, T. Zhu, Q. Zhang, W. Hou, W. Z. Yuan, *Chem. Soc. Rev.* **2021**, *50*, 12616.
[45] H. Zhang, Z. Zhao, P. R. Mcgonigal, R. Ye, S. Liu, J. W. Y. Lam, R. T. K. Kwok, W. Z. Yuan, J. Xie, A. L. Rogach, B. Z. Tang, *Mater. Today* **2020**, *32*, 275.
[46] Y. Wang, Z. Zhao, W. Z. Yuan, *ChemPlusChem* **2020**, *85*, 1065.
[47] L.i X. Hou, H. Ju, X. P. Hao, H. Zhang, L. Zhang, Z. He, J. Wang, Q. Zheng, Z.i L. Wu, *Adv. Mater.* **2023**, *35*, 2300244.
[48] H. Ju, H. Zhang, L.i X. Hou, M. Zuo, M. Du, F. Huang, Q. Zheng, Z.i L. Wu, *J. Am. Chem. Soc.* **2023**, *145*, 3763.
[49] T. Liu, C. Jiao, X. Peng, Y.a-N. Chen, Y. Chen, C. He, R. Liu, H. Wang, *J. Mater. Chem. B* **2018**, *6*, 8105.
[50] R. Ricciardi, F. Auriemma, C. De Rosa, F. Lauprêtre, *Macromolecules* **2004**, *37*, 1921.
[51] Y. Wu, T. Liu, Y. Shi, H. Wang, *Polymer* **2022**, *249*, 124842.
[52] D. Li, Y. Yang, J. Yang, M. Fang, B. Z. Tang, Z. Li, *Nat. Commun.* **2022**, *13*, 347.
[53] J. Zhang, M. Dolg, *Phys. Chem. Chem. Phys.* **2015**, *17*, 24173.
[54] J. Zhang, M. Dolg, *Phys. Chem. Chem. Phys.* **2016**, *18*, 3003.
[55] J. Zhang, *J. Chem. Phys.* **2022**, *156*, 204108.
[56] M. J. Frisch, G. W. Trucks, H. B. Schlegel, G. E. Scuseria, M. A. Robb, J. R. Cheeseman, G. Scalmani, V. Barone, G. A. Petersson, H. Nakatsuji, X. Li, M. Caricato, A. V. Marenich, J. Bloino, B. G. Janesko, R. Gomperts, B. Mennucci, H. P. Hratchian, J. V. Ortiz, A. F. Izmaylov, J. L. Sonnenberg, Williams, F. Ding, F. Lipparini, F. Egidi, J. Goings, B. Peng, A. Petrone, T. Henderson, D. Ranasinghe, et al., *Gaussian 16, Revision A.03*, Gaussian, Inc., Wallingford, CT **2016**.
[57] F. Neese, *WIREs: Comput. Mol. Sci.* **2018**, *8*, e1327.
[58] C. Adamo, V. Barone, *J. Chem. Phys.* **1999**, *110*, 6158.
[59] F. Weigend, R. Ahlrichs, *Phys. Chem. Chem. Phys.* **2005**, *7*, 3297.
[60] R. Ditchfield, W. J. Hehre, J. A. Pople, *J. Chem. Phys.* **1971**, *54*, 724.
[61] M. M. Francl, W. J. Pietro, W. J. Hehre, J. S. Binkley, M. S. Gordon, D. J. Defrees, J. A. Pople, *J. Chem. Phys.* **1982**, *77*, 3654.
[62] M. S. Gordon, J. S. Binkley, J. A. Pople, W. J. Pietro, W. J. Hehre, *J. Am. Chem. Soc.* **1982**, *104*, 2797.
[63] W. J. Hehre, R. Ditchfield, J. A. Pople, *J. Chem. Phys.* **1972**, *56*, 2257.
[64] V. A. Rassolov, M. A. Ratner, J. A. Pople, P. C. Redfern, L. A. Curtiss, *J. Comput. Chem.* **2001**, *22*, 976.